

# Composition Studies with the Pierre Auger Observatory

M. Unger <sup>a</sup> for the Pierre Auger Collaboration <sup>b</sup>

<sup>a</sup> Karlsruhe Institut für Technologie (KIT)  
Postfach 3640, D-76021 Karlsruhe, Germany

<sup>b</sup>Observatorio Pierre Auger  
Av. San Martin Norte 304, 5613 Malargüe, Argentina

We report on studies of the composition of ultra high energy cosmic rays with the Pierre Auger Observatory. The detection of longitudinal air shower profiles with the fluorescence detector is described and the measurement of the average shower maximum as a function of energy is presented. Furthermore, mass sensitive parameters that can be obtained from the observatory's surface detector data are discussed.

## 1. Introduction

The Pierre Auger Observatory is a facility to study the origin of ultra high energy cosmic rays by a combined measurement of their flux, anisotropy and mass composition.

The southern site of the observatory is located near the town of Malargüe in Argentina and its construction has been completed at the end of 2008. Even during its assembly, data have been collected in a stable manner since January 2004. The lateral densities of charged air shower particles at ground level are measured with the surface detector (SD), an array of 1600 water Cherenkov detectors distributed on an area of 3000 km<sup>2</sup>. In addition, the longitudinal air shower development can be observed with the fluorescence detector (FD), consisting of 24 wide-angle Schmidt telescopes that overlook the atmospheric volume above the surface detector.

The mass composition of cosmic rays above 10<sup>17</sup> eV is a key observable to discriminate between different models put forward to explain the softening of the cosmic ray energy spectrum at energies between 10<sup>18</sup> and 10<sup>19</sup> eV (the so called 'ankle', see [2] for a recent review). Moreover, a measurement of the ultra high energy cosmic ray composition is essential to understand the nature of the flux suppression observed above 5·10<sup>19</sup> eV [1].

In this article we will explain, how the cosmic ray composition can be inferred from air

shower measurements with the Pierre Auger Observatory. An estimate of the primary composition from the measurement of the longitudinal air shower profiles with the fluorescence detector will be given in the next section, followed by the description of the mass sensitive observables of the surface detector.

## 2. Fluorescence Detector Measurements

Within the Heitler model [4] of cosmic ray induced particle cascades, the maximum number of electromagnetic particles of a shower with energy  $E$  and mass  $A$  is reached at a depth of

$$\langle X_{\max} \rangle = \alpha + X_0 (\ln E - \langle \ln A \rangle) \quad (1)$$

where  $X_0$  denotes the electromagnetic radiation length in air. The details of the hadronic interactions feeding the shower are subsumed into the parameter  $\alpha = \lambda \ln 2 - X_0 \ln(3N_{\text{ch}}E_{\text{crit}})$ , where  $\lambda$  denotes the hadronic interaction length,  $N_{\text{ch}}$  is the charged particle multiplicity and  $E_{\text{crit}}$  the energy threshold, below which ionization becomes more important than radiative processes. The change of  $X_{\max}$  per logarithm of energy is called elongation rate [3]:

$$D = \frac{d\alpha}{d \ln E} + X_0 \left( 1 - \frac{d \langle \ln A \rangle}{d \ln E} \right). \quad (2)$$

Thus, given a prediction of  $\alpha$  and  $\frac{d\alpha}{d \ln E}$  from air shower simulations, the primary mass composition can be estimated from the average shower

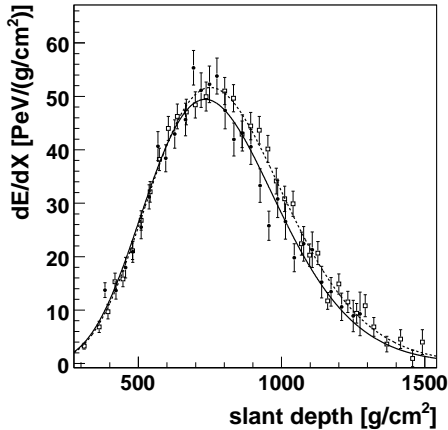


Figure 1. Example of a measured longitudinal profile, reconstructed independently by two fluorescence detectors: Los Leones (black dots,  $E=31\pm 2$  EeV,  $X_{\max}=733\pm 18$  g/cm $^2$ ) and Los Morados (open squares,  $E=33\pm 2$  EeV,  $X_{\max}=751\pm 16$  g/cm $^2$ ).

maximum  $\langle X_{\max} \rangle$  and its relative change with energy from the elongation rate. In the following we will describe the measurement of these two quantities with the Auger fluorescence detector.

### 2.1. Event Reconstruction

In the FD composition analysis only events recorded in hybrid mode [5] are considered, i.e. the shower development must have been measured by the fluorescence detector and at least one coincident SD station is required to provide a ground level time that is needed for a precise determination of the shower direction. The longitudinal energy deposit profile is reconstructed [6] from the light recorded by the FD using the fluorescence and Cherenkov yields from [7] and [8]. With the help of data from the observatory's atmospheric monitoring devices [9] the attenuation of the light on its way from the shower to the detector is corrected for and the measured light emission heights are converted to atmospheric depth. Fig. 1 shows an example of a reconstructed longitudinal profile of an air shower, that trig-

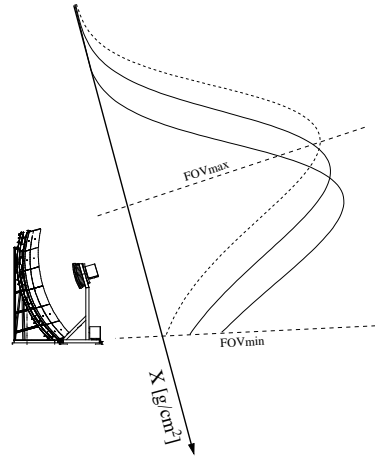


Figure 2. Sketch of the field of view of a fluorescence telescope and three longitudinal profiles. Showers with their maximum above FOVmax or below FOVmin are not selected.

gered two of the four Auger fluorescence detectors. The data is fitted with a Gaisser-Hillas function [10] to extrapolate the profile to depths outside the field of view of the fluorescence telescopes. The integral over this function gives the calorimetric energy of the shower and the depth where it is maximal is at  $X_{\max}$ . From showers that were observed simultaneously by more than one fluorescence detector, the difference in the reconstructed shower parameters can be used to infer the resolution of the  $X_{\max}$  reconstruction. It is about 20 g/cm $^2$ .

### 2.2. Field of View Bias

The energy and shower maximum can only be reliably measured, if  $X_{\max}$  is in the field of view of the telescopes (otherwise only the rising or falling edge of the profile is detected). As illustrated in Fig. 2, this may lead to a biased event selection, if both, events with a small or large  $X_{\max}$ , are not included in the analysis because of their poor reconstruction. The current Auger fluorescence detectors cover an elevation range from  $\Omega_1 = 1.5^\circ$  to  $\Omega_2 = 30^\circ$  and therefore the observable heights for vertical tracks are between  $R \tan \Omega_1 < h_v < R \tan \Omega_2$ , where  $R$  denotes the

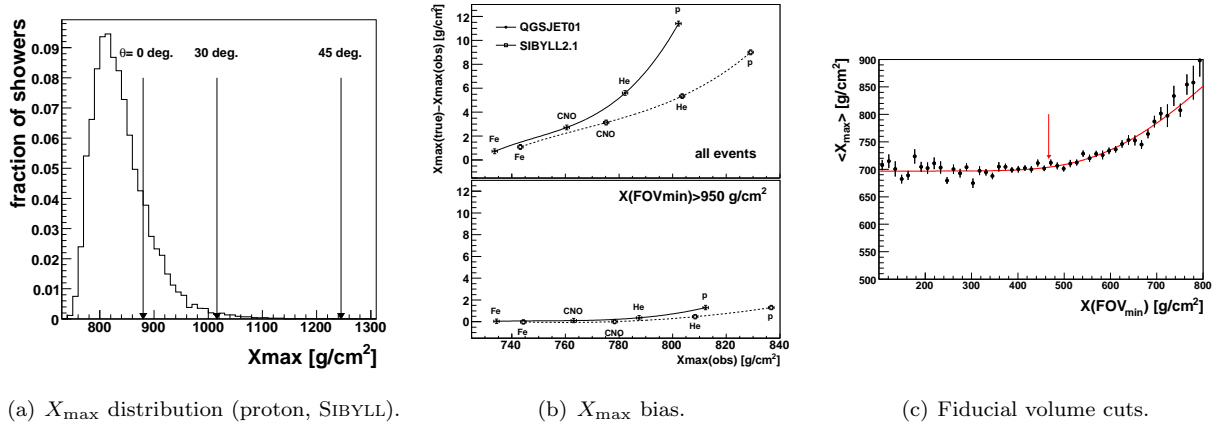


Figure 3. Field of view bias. Left and middle panel: Air shower simulations at  $E=10^{19.5}$  eV. Right panel: Data at  $10^{18}$  eV  $< E < 10^{18.25}$  eV.

distance of the shower core to the fluorescence detector. That is, the farther away from a fluorescence detector a track is detected, the smaller becomes the observable upper slant depth boundary  $X(\text{FOV}_{\min})$ . Similarly the lower slant depth boundary  $X(\text{FOV}_{\max})$  becomes larger for near showers.

The absolute magnitude of the field of view bias depends of course on the, a priori unknown, distribution of the depth of shower maxima of cosmic ray showers. It is instructive to study the order of magnitude of the field of view bias for simulated showers with a known composition. The expected  $X_{\max}$  distribution for protons with an energy of  $10^{19.5}$  eV is shown in Fig. 3(a). The upper viewable slant depth limits are indicated as arrows for different zenith angles. For vertical tracks it is around  $880$  g/cm<sup>2</sup> at the southern observatory, which is obviously not sufficient to detect the full  $X_{\max}$  distribution. A convolution of the truncated  $X_{\max}$  distributions with the arrival directions of isotropic cosmic rays ( $dN/d\cos\theta \propto \cos\theta$ ) leads to an effective bias for the measurement of the mean of the distribution. As can be seen in the upper panel of Fig. 3(b), this bias can be as large as  $12$  g/cm<sup>2</sup>. Due to the unknown composition and the theoretical uncertainties of air shower simulations it can not be corrected for a posteriori, since there is no unambiguous correc-

tion given a measured  $\langle X_{\max} \rangle$ .

The strategy followed in this analysis is therefore to ignore showers that have a too small viewable slant depth range. The rejection of showers with  $X(\text{FOV}_{\min}) < 950$  g/cm<sup>2</sup> almost completely removes the bias on  $\langle X_{\max} \rangle$  in the simulation, cf. lower panel of Fig. 3(b). The *fiducial volume cuts* that ensure an unbiased  $\langle X_{\max} \rangle$  can be derived directly from data as illustrated in Fig. 3(c): The dependence of  $\langle X_{\max} \rangle$  on the slant depth boundaries is studied and events are only selected in the region where  $\langle X_{\max} \rangle$  is constant.

### 2.3. Results

The  $\langle X_{\max} \rangle$  results presented here were derived from hybrid data recorded between December 2004 and April 2007. In order to ensure a good  $X_{\max}$  resolution, the following quality cuts were applied to the event sample: The reconstructed  $X_{\max}$  should lie within the observed shower profile and the reduced  $\chi^2$  of a fit with a Gaisser-Hillas function should not exceed 2.5. Moreover, insignificant shower maxima are rejected by requiring that the  $\chi^2$  of a linear fit to the longitudinal profile exceeds the Gaisser-Hillas fit  $\chi^2$  by at least four. Finally, the estimated uncertainties of the shower maximum and total energy must be smaller than  $40$  g/cm<sup>2</sup> and  $20\%$ , respectively. Moreover, the fiducial volume cuts explained in

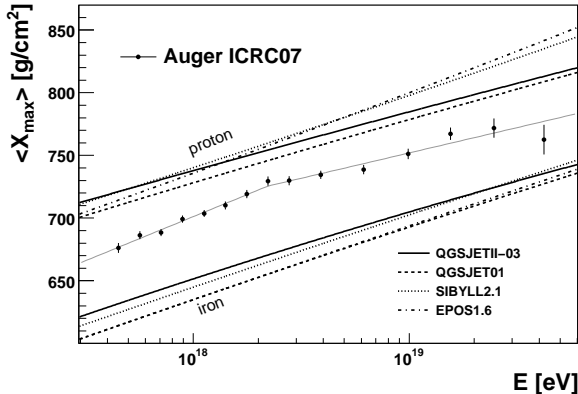


Figure 4.  $\langle X_{\max} \rangle$  as a function of energy [14].

the last section are applied.

The systematic uncertainties of the atmospheric properties, event reconstruction and mass acceptance add up to a total estimated systematic uncertainty of  $\langle X_{\max} \rangle$  that is  $\lesssim 15$  g/cm<sup>2</sup> at low energies and  $\lesssim 11$  g/cm<sup>2</sup> above  $10^{18}$  eV.

In Fig. 4 the mean  $X_{\max}$  as a function of energy is shown along with predictions from air shower simulations [11]. As can be seen, the measurement favors a mixed composition at all energies.

A simple linear fit, yields an elongation rate of  $54 \pm 2$  (stat.) g/cm<sup>2</sup>/decade, but does not describe our data very well ( $\chi^2/\text{Ndf} = 24/13$ ,  $P < 3\%$ ). Allowing for a break in the elongation rate at an energy  $E_b$  leads to a satisfactory fit with  $\chi^2/\text{Ndf} = 9/11$ ,  $P = 63\%$  and  $D_{10} = 71 \pm 5$  (stat.) g/cm<sup>2</sup>/decade below  $E_b = 10^{18.35}$  eV and  $D_{10} = 40 \pm 4$  (stat.) g/cm<sup>2</sup>/decade above this energy. This fit is indicated as a gray line in Fig. 4.

Due to the uncertainties of hadronic interaction at highest energies, the interpretation of these elongation rates is, however, ambiguous. Using QGSJETII the data suggests a moderate lightening of the primary cosmic ray composition at low energies and an almost constant composition at high energies, whereas the EPOS proton elongation rate is clearly larger than the measured one at high energies, which would indicate a transition from light to heavy elements. These ambi-

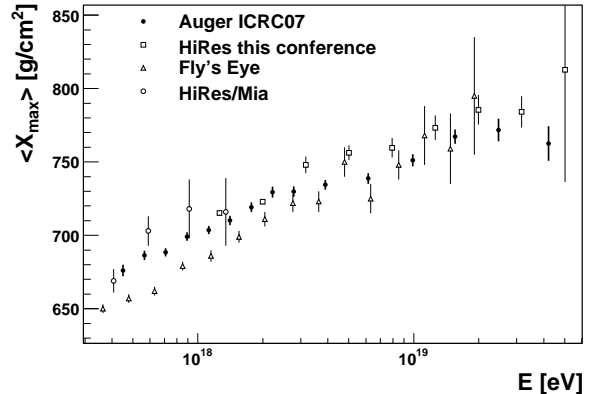


Figure 5. Comparison to  $\langle X_{\max} \rangle$  from other experiments [12, 13].

guities will be partially resolved by the analysis of the  $X_{\max}$  fluctuations as an additional mass sensitive parameter.

A comparison with measurements of other experiments is presented in Fig. 5. Taking into account the individual systematic uncertainties of each experiment there is a reasonable agreement of the  $\langle X_{\max} \rangle$  values. It is, however, worthwhile noting that HiRes uses a different definition of  $X_{\max}$  (see [13]) that is about 10 g/cm<sup>2</sup> shallower than the one commonly used (depth of non-parametric shower maximum). If this is taken into account, the elongation rates of Auger and HiRes show a discrepancy in the  $X_{\max}$ -scale of about 30 g/cm<sup>2</sup>.

### 3. Surface Detector Measurements

As we have explained in the last section, the longitudinal air shower development is a good tracer for the primary composition that can be measured very precisely with fluorescence telescopes. However, these telescopes can only take data in moonless nights, whereas the surface detector has a duty cycle of almost 100% and correspondingly, the available event statistics are about a factor ten higher. Because of this, and the obviously independent systematic uncertain-

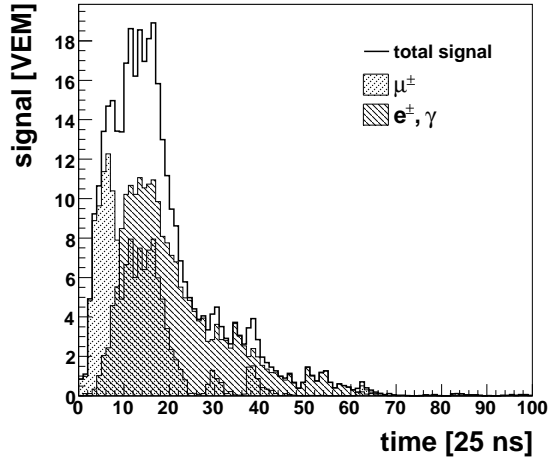


Figure 6. Simulated air shower signal in a water Cherenkov detector

ties, it is worthwhile to study ground level observables that are sensitive to the primary composition as well.

Since the amount of electromagnetic particles at ground depends for a given energy on the distance to the shower maximum it depends also on the primary mass. Moreover, the number of ground level muons evolves differently with energy for different primary masses. From the Heitler model one expects

$$N_{\mu} \propto E^{\beta} A^{1-\beta} \quad (3)$$

where  $\beta$  depends on the multiplicity and inelasticity of hadronic interaction (and is thus, as the above  $\alpha$ , subject to theoretical uncertainties). Since the water Cherenkov detectors of the Pierre Auger Observatory cannot explicitly discriminate between the electromagnetic and muonic air shower components on an event by event basis (but see Sec. 4), a variety of 'indirect' experimental variables are currently investigated to relate the surface detector data to the primary mass [22]: The signal rise time, its asymmetry and the signal shape analysis<sup>1</sup>.

<sup>1</sup>For yet another composition sensitive parameter, the shower front curvature, see [21].

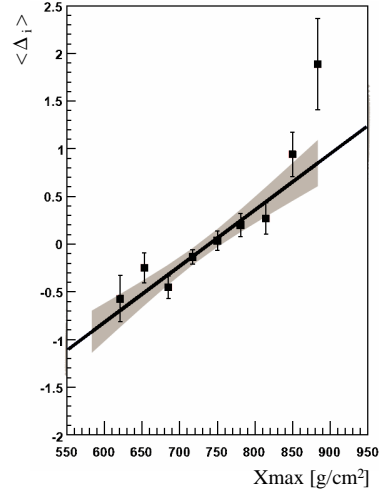


Figure 7. Correlation of rise time and  $X_{\max}$

### 3.1. Risetime

For each event, the water Cherenkov detectors record the signal as a function of time (FADC traces). This provides a possibility to distinguish the muonic and electromagnetic component, since the former travel in almost straight lines through the atmosphere, whereas the latter undergo multiple scattering on their way to ground. Therefore, the two components have different path lengths and arrival times at ground. This is illustrated in Fig. 6, where an example of a simulation [15, 16] of the surface detector response is shown. The *rise time*  $t_{1/2}$  [17] is the time it takes until the cumulative signal grows from 0.1 to 0.5. It is a measure of the muon to electron ratio in a tank and depends on the primary mass, angle of incidence  $\theta$  and distance to the shower core  $r$ . The  $r$  and  $\theta$  dependence is marginalized by a comparison to the average rise time  $\langle t_{1/2}(\theta, r) \rangle$  and the pull  $\Delta_i = (t_{1/2} - \langle t_{1/2}(\theta, r) \rangle) / \sigma(t_{1/2})$  is averaged over the stations of an event to yield  $\langle \Delta_i \rangle$  [19]. This quantity could in principle be compared to air shower simulations. However, as previous studies showed, the number of muons measured in Auger can not be reproduced by these calculations [18]. Therefore, instead of a direct comparison of  $\langle \Delta_i \rangle$  to air shower simula-

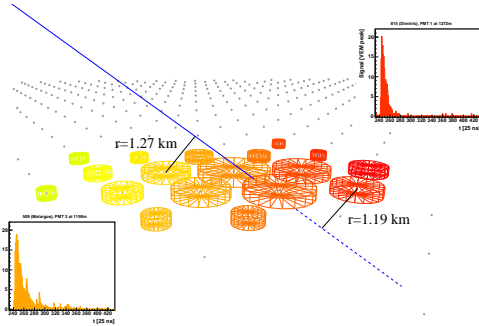


Figure 8. Asymmetry of station signals ( $\theta=54^\circ$ ,  $E=55\pm 2$  EeV)

tions, it is related to the shower maximum. For this purpose, the subset of events that have been detected by both, the fluorescence and surface detector, are used to establish the relation between  $\langle\Delta_i\rangle$  and  $X_{\max}$ . As can be seen in Fig. 7, there is a linear correlation between the two variables, with which the surface detector data can be calibrated to yield  $X_{\max}(\langle\Delta_i\rangle)$ , with which it is possible to measure the elongation rate with surface detector data.

### 3.2. Risetime Asymmetry

The SD stations measure one stage of the shower development for near vertical events. In case of inclined showers, however, considerably different shower ages can be observed, depending on whether the station is up- or downstream of the incoming shower direction. This is illustrated in Fig. 8, where the signal traces of two stations (both at the same shower plane distance  $r$ ) are shown. The upstream trace is rather broad, which is compatible with a large fraction of electromagnetic particles. The downstream trace is narrower indicating that most of the electromagnetic component has been attenuated and the signal is dominated by muons. The corresponding *asymmetry* [20] in the rise time is thus a measure of the longitudinal development of the ratio

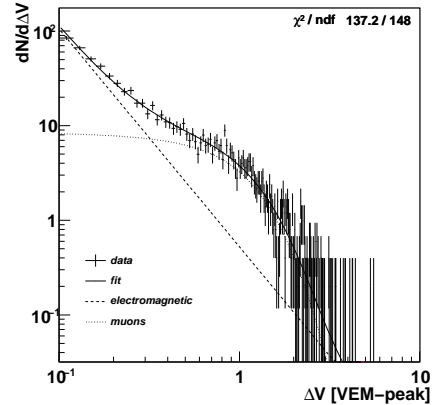


Figure 9. Distribution of jumps for events at a given energy, zenith angle and distance to the core range.

of electromagnetic to muonic particles. The amplitude of the asymmetry changes with the zenith angle, i.e. distance to the shower maximum. The angle at which it reaches its maximum can be used as an estimator for the primary composition.

### 3.3. Signal Shape

Since a muon deposits much more energy (typically 240 MeV) in a water tank than an electron or photon (about 10 MeV), spikes are produced over the smoother electromagnetic background in the FADC time traces. Therefore, muons can be identified by searching for sudden variations, in the signal from one FADC bin to the next (cf. Fig 6). The expected distributions of variations for purely electromagnetic and muonic traces can be fitted to the measured distribution as shown in Fig. 9. In that way, the muonic signal can be determined on a statistical basis with a resolution of about 25% and the number of muons as a function of energy can be compared to predictions from air shower simulations to estimate the primary composition.

## 4. Conclusions and Outlook

In this article we presented the measurement of the elongation rate from data collected with the

fluorescence telescopes of the Pierre Auger Observatory. When compared to predictions from air shower simulation the  $\langle X_{\max} \rangle$  data favors a mixed composition at all energies. This measurement will be soon updated with larger statistics and an analysis of the fluctuations of the shower maximum. At lower energies the systematic uncertainties will be reduced by additional telescopes that cover the field of view from 30 to 60 degree [23]. A variety of surface detector observables are sensitive to the mass composition. These parameters have a somewhat worse mass resolution than  $X_{\max}$ , which is, however, outweighed by the large event statistics collected by the ground array. Due to the hybrid design of the Pierre Auger Observatory, the correlation between the lateral and longitudinal shower parameters can be studied and additional muon detectors will soon allow for an event-by-event measurement of the muon content of a shower [24].

## REFERENCES

1. J. Abraham et al. [Pierre Auger Coll.], *Phys. Rev. Lett.*, 101:061101, 2008; R. Abbasi et al. [HiRes Coll.], *Phys. Rev. Lett.*, 100:101101, 2008.
2. V. Berezhinsky, Proc. 30th ICRC (2007), arXiv:0710.2750 [astro-ph].
3. J. Linsley and A.A. Watson, *Phys. Rev. Lett.* **46** (1981), 459; T.K. Gaisser et al., Proc. 16th ICRC **9** (1979), 258; J. Linsley, Proc. 15th ICRC **12** (1977), 89.
4. J. Matthews, *Astropart. Phys.* **22** (2005), 387; W. Heitler, Oxford Univ. Press, 1954.
5. P. Sommers, *Astropart. Phys.* **3** (1995), 349.
6. M. Unger et al., *Nucl. Instrum. Meth.* **A588** (2008), 433; B. Dawson, M.Giller and G. Wieczorek, Proc. 30th ICRC (2007); D. Gora et al., *Astropart. Phys.* **24** (2006), 484; M. D. Roberts, *J. Phys.* **G31** (2005), 1291;
7. M. Ave et al. [AIRFLY Coll.], *Astropart. Phys.* **28**, (2007) 41; M. Nagano et al., *Astropart. Phys.* **22** (2004), 235.
8. F. Nerling et al., *Astropart. Phys.* **24** (2006), 421.
9. S. Y. BenZvi for the Pierre Auger Coll., Proc. 30th ICRC (2007); B. Keilhauer for the Pierre Auger Coll., Proc. 29th ICRC **7** (2005), 123.
10. T. K. Gaisser and A. M. Hillas, Proc. 15th ICRC **8** (1977), 353.
11. T. Bergmann et al., *Astropart. Phys.* **26** (2007) 420; N. N. Kalmykov, S. S. Ostapchenko and A. I. Pavlov, *Nucl. Phys. Proc. Suppl.* **52B** (1997) 17; R. Engel, T. K. Gaisser, T. Stanev and P. Lipari, Proc. 26th ICRC (1999), 415; S. Ostapchenko, *Nucl. Phys. Proc. Suppl.* **151** (2006) 143; T. Pierog and K. Werner, *Phys. Rev. Lett.* **101** (2008) 171101.
12. D.J. Bird et al. [HiRes Coll.], *Phys. Rev. Lett.* **71** (1993), 3401; T. Abu-Zayyad et al. [HiRes/MIA Coll.], *Astrophys. J.* **557**, (2001), 685.
13. J. Belz for the HiRes Coll., these proceedings.
14. M. Unger for the Pierre Auger Coll., Proc. 30th ICRC, Merida (2007), arXiv:0706.1495 [astro-ph].
15. S. Argiro *et al.*, *Nucl. Instrum. Meth. A* **580** (2007) 1485
16. D. Heck, G. Schatz, T. Thouw, J. Knapp and J. N. Capdevielle, FZKA-6019 (1998)
17. R. Walker and A.A. Watson, *J. Phys. G* **7** (1981), 1297.
18. R. Engel for the Pierre Auger Coll., Proc. 30th ICRC (2007), arXiv:0706.1921 [astro-ph].
19. B. E. Smith, PhD Thesis University of Leeds (2008).
20. M.T. Dova for the Pierre Auger Coll., Proc. 29th ICRC (2005), arXiv:astro-ph/0507171
21. M. Risse for the Pierre Auger Coll., these proceedings, arXiv:0901.2525 [astro-ph].
22. M.D. Healy for the Pierre Auger Coll., Proc. 30th ICRC (2007), arXiv:0706.1569 [astro-ph].
23. H. O. Klages for the Pierre Auger Coll., Proc. 30th ICRC, (2007).
24. A. Etchegoyen for the Pierre Auger Coll., Proc. 30th ICRC, (2007), arXiv:0710.1646 [astro-ph].